Alma Mater Studiorum Università di Bologna
Archivio istituzionale della ricerca

Identification of the inertial parameters of underactuated Cable-Driven Parallel Robots

(Article begins on next page)

25 April 2024

Identification of the Inertial Parameters of Underactuated Cable-Driven Parallel Robots

Edoardo Idà[a,*], Sébastien Briot[b], and Marco Carricato[a]

[a] *Dept. of Industrial Engineering, University of Bologna, 40137 Bologna, Italy*
[b] *Centre National de la Recherche Scientifique (CNRS) at the Laboratoire des Sciences du Numérique de Nantes (LS2N), UMR CNRS 6004, 44300 Nantes, France*

Abstract

Cable-Driven Parallel Robots (*CDPR*) employ extendable cables to control the pose of an end-effector (*EE*). If the number of cables is smaller than the degrees of freedom of the *EE*, and cables have no special arrangement reducing the *EE* freedoms, the robot is underactuated, and the *EE* is underconstrained: as a consequence, the *EE* preserves some freedoms even when all actuators are locked, which may lead to undesirable free motions. This paper proposes a novel methodology for the identification of the *EE* inertial parameters of these robots. Inertial parameters are useful, for example, in the application of feedforward control techniques. The main merit of our approach is that it does not require force or torque measurements, and only a subset of the robot kinematic variables needs to be measured. The method consists in the application of the *EE* internal-dynamics equations along a free-motion trajectory, also referred to as self-motion zero dynamics. This results in an over-determined system of equations that are linear in the *EE* inertial parameters (the Free-motion Internal-Dynamics Identification Model, *FIDIM*); the said system is solved according to the Total-Least-Square technique. Free-motion trajectories that are optimal for identification purposes are investigated and experimentally tested on a 4-cable robot. *FIDIM* is then applied, statistical analysis is performed, and the experimental results are cross-validated against additional free-motion trajectories.

Keywords: Underactuated robots, underconstrained robots, cable-driven parallel robots, inertial parameter estimation.

1. Introduction

A cable-driven parallel robot (*CDPR*) is a parallel manipulator that employs cables, instead of rigid-link legs, to move an end-effector (*EE*). A *CDPR* equipped with a μ-*DoF EE* and n actuated cables, with $n < \mu$, is generally underactuated[1], and only a subset of the *EE* coordinates

---

*Corresponding author
    Email address:* `edoardo.ida2@unibo.it` (Edoardo Idà)
    [1] There may be special cable arrangements on the *EE* that may reduce the *EE* freedoms and, thus, may result in the robot being fully actuated [1].

can be controlled directly, with the remaining ones being determined by the system mechanical equilibrium. An underactuated *CDPR* (*UACDPR* in short) is always underconstrained, thus its *EE* preserves mobility even if its actuators are locked [2]. Accordingly, if the *EE* is not in a static configuration when cable lengths are not varying, it exhibits (possibly dangerous) oscillatory *free motions* in the Cartesian space [3]. The Cartesian free motions of an underactuated parallel robot, which occur when actuators are locked, are conceptually analogous to the joint-space self motions of overactuated serial robots, which may occur when the *EE* is fixed [4].

 UACDPR may be employed in a variety of applications, in which a simpler mechanical system and enhanced workspace accessibility justify limited robot mobility and controllability [5–7]. Thus, the study of *UACDPRs* is attracting the interest of more and more researchers, who have dealt with geometrico-static problems [8, 9], equilibrium stability analysis [10, 11], trajectory planning [2, 12–18], system-parameter identification [3, 19], performance evaluation [20], and control [21–24].

 In order to limit *EE* oscillations during motion, feedforward [2, 17, 18] controllers based on *EE* dynamics can be employed: in this case, the system inertial parameters must be known. They may be estimated by means of *CAD* tools or, if high accuracy is needed in their evaluation, they must be *identified*. Classical inertial-parameter identification models aim at determining the mass of the moving links, the position of their centers of mass, and their inertia matrices with respect to (w.r.t. in short) to some body-fixed frames. In addition, the actuators inertia, friction coefficients, and their drive current gains can also be determined [25]. The need of a precise identification of the *EE* inertial parameters in an *UACDPR* is especially justified if a feed-forward control scheme, with cable length as a system input, is used. In fact, the computation of actuator position set-points relies on the evaluation of the robot non-controllable freedoms while following a prescribed trajectory of the controlled ones [2, 13, 17, 18]: the non-controllable freedoms are found by numerically integrating the *EE* internal dynamics, which is influenced by the inertial parameters of the *EE*, which are thus the *EE base parameters* [26].

 In the field of cable-driven robots, standard [27, 28] or simplified [29] identification methodologies were applied to redundantly-actuated *CDPRs* or single winches [30]. The authors of [27, 28] employed an *Output-Error Identification Method*, based on the direct dynamic model, for the identification of both actuator and *EE* inertial parameters of an over-constrained *CDPR*. The proposed method results in an overdetermined system of nonlinear equations, which require actuator positions, actuator torques, and the *EE* pose to be experimentally measured or estimated. The *EE* inertial parameters of an over-constrained *CDPR* were identified in [29] according to a two-step cascaded *Inverse-Dynamics Identification Model*, where the inertia matrix is found after the *EE* mass and center-of-mass position are identified first. The identification model proposed in [29] is linear, thus computationally simpler than the output-error method, but it requires additional inputs, such as the *EE* angular velocity and acceleration, and the *EE* linear acceleration, obtained by means of an inertial measurement unit; moreover, since actuator dynamics is not taken into consideration, cable tensions are directly measured by force sensors. A drawback is that, due to the cascaded nature of the identification model, errors in the identification of the first group of parameters cumulate with those of the second group. In [30] the authors focused on the identification of winch parameters (in the frequency domain), whose dynamics was modelled as a discrete-time second-order spring-mass-damper: the identification was carried out by measuring motor positions and cable forces.

2

A few studies also exist on identification of *EE* parameters in robotic systems which are practically coincident to *UACDPRs* [31–34], even though their target application is inertial-parameter measurement per-se. The authors of [31–34] developed and studied an instrumentation for the precise measurement of inertial parameters of a suspended body; the instrumentation employs 3 or 4 fixed-length cables, attached to the fixed frame and the mobile platform by universal joints. Thanks to this set-up, encoders on the universal joints connecting the cables to the frame allow the measurement of the cable angular position and ultimately the estimation of the *EE* pose. Additionally, an axial force sensor, embedded between each universal joint and each cable, measures the cable tension, which is required by the adopted identification method. One of the most notable innovations of [31–34] is the use of the *EE* free motion as excitation trajectory for identification: this makes the instrumentation simpler (cables do not need to be actuated), and avoids the computation of (possibly) complicated exciting trajectories, which are required by standard techniques [28, 29].

As detailed above, most of the strategies proposed in the literature to identify robot inertial parameters present common theoretical aspects, such as [35]:

- a dynamic model that is linear in the inertial parameters is formulated, so that parameters can be algebraically isolated;

- an over-determined linear system of equations is obtained, by applying the dynamic model to a sufficient number of configurations along some trajectory of the robot;

- inertial parameters are determined by using linear regression techniques.

On the practical side, additional considerations often lead to identification best practices:

- identifiability of inertial parameters can be investigated, so that non-identifiable or non-essential ones are eliminated from the dynamic model [35]; in fact, when a parameter is intrinsically not identifiable or non-essential, it has a minimal influence on the dynamic model: by eliminating it, identifiable parameters are estimated with higher precision and the dynamic model is simplified;

- robot trajectories for identification should be optimal with respect to some identifiability criterion, in order to increase the accuracy of the regression analysis;

- after parameters are identified, statistical-error-analysis tools should be employed to draw conclusions on the experimental results: in case statistical errors are large, experiments should be disregarded and re-performed.

This paper proposes a novel methodology for the identification of *UACDPR EE* inertial parameters. The main contributions are the following.

1. The method takes advantage of the internal dynamics and free-motion kinematics (that is, a zero dynamics [36, 37]) of the underactuated *EE*; in this way, contrary to state-of-the-art identification procedures for *CDPRs* [28, 29, 31], force or torque measurements are avoided, and only a subset of the *EE* coordinates needs to be measured or estimated. This feature is particularly beneficial for two reasons, since it avoids (i) the integration of expensive sensing equipment, and (ii) the use of their (usually) noisy data for identification. Pulley and actuator friction parameters, as well as actuator inertia, are not estimated and would require methods similar to [28, 29], but *EE* inertial parameters are sufficient for most feedforward control techniques used for *UACDPR* [2, 13, 17, 18].

3

2. The application of the internal-dynamics equations along a free-motion trajectory provides an over-determined system of linear equations, the Free-Motion Internal-Dynamics Identification Model (*FIDIM*), which is solved according to the Total-Least-Square (*TLS*) method [38]. The *TLS* method provides an optimal solution by minimizing both modelling and measurements errors, compared to Least-Square or Output-Error methods, which only minimize modelling errors [39].

3. Optimal free-motion trajectories are investigated, and extensive simulations show that randomly exciting *EE* oscillations about different equilibria may be sufficient for obtaining optimal identification results. This means that there is possibly no need to calculate complex optimal excitations.

The rest of the paper is structured as follows. Section 2 presents *UACDPRs* models, with a focus on internal dynamics and free-motion kinematics. Section 3 establishes the novel *FIDIM*, and introduces its solution technique: the Total-Least-Square method. An optimal free-motion excitation strategy is introduced in Sec. 4, and applied in Sec. 5, where identification experiments, and their results, are discussed. Conclusion and outlook are finally reported in Sec. 6.

2. *UACDPR* Modelling

This Section briefly presents the kinematic and dynamic models of an *UACDPR*. The content is drawn from [2, 3], and it is succinctly reported here only to introduce the nomenclature and the equations that are necessary for the subsequent development. An *UACDPR* consists of a mobile platform coupled to the base by n cables, with $n < \mu$, and $\mu = 6$ in $SE(3)$. Cables can be coiled and uncoiled by motorized winches. $Oxyz$ is an inertial frame, whereas $Px'y'z'$ is a mobile frame attached to the *EE*, whose pose is described by the position vector $\mathbf{p}$ of P, and a rotation matrix $\mathbf{R}$, parametrized by a minimal set of orientation parameters $\boldsymbol{\epsilon}$, namely $\mathbf{R} = \mathbf{R}(\boldsymbol{\epsilon})$. *EE* generalized coordinates are denoted by $\boldsymbol{\zeta} = \left[\mathbf{p}^T \boldsymbol{\epsilon}^T\right]^T$.

2.1. UACDPR geometry

Each cable is guided into the workspace by a swivel pulley, mounted on an hinged support. Each cable enters the pulley in point D_i, that lies on the swivel axis, tangentially exits the pulley in point B_i, and is attached to the *EE* in point A_i. $\mathbf{a}_i$ and $\mathbf{a}'_i$ are the position vectors of A_i w.r.t. O and P, respectively. $\mathbf{b}_i$ denotes the position of B_i w.r.t. O and, if pulley kinematics is accounted for, depends on the *EE* pose [2] (Fig. 1). If cables are assumed to be massless and inextensible[2], the constraint imposed by each cable onto the *EE* is:

$$\boldsymbol{\rho}_i^T \boldsymbol{\rho}_i - \left[l_i - \widehat{B_i D_i}\right]^2 = 0 \qquad (1)$$

where $\boldsymbol{\rho}_i \overset{\Delta}{=} \mathbf{a}_i - \mathbf{b}_i$, and l_i is the total cable length, comprising the rectilinear part $\|\boldsymbol{\rho}_i\|$ and the arc $\widehat{B_i D_i}$ wrapped onto the pulley.

---

[2]These assumptions are reasonable if the robot is small- to medium-size, and employs polymer-fibre cables, such as the prototype used for the experiments reported in Section 5.
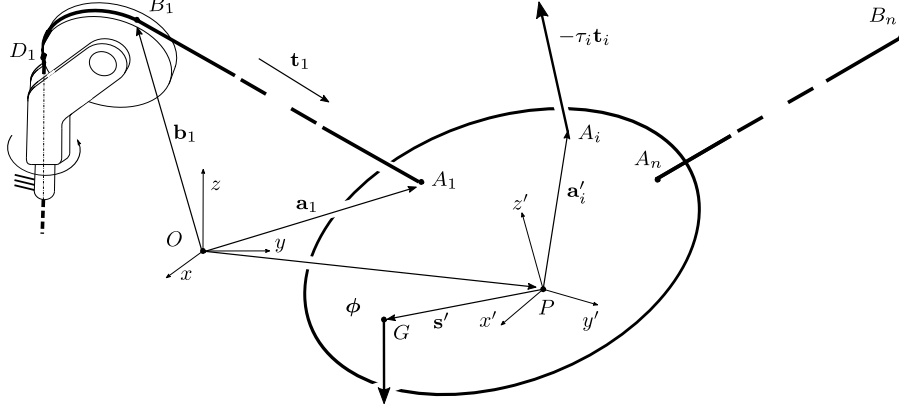
Figure 1: EE *Free-Body Diagram*

2.2. UACDPR free-motion kinematics

If $\boldsymbol{\omega}$ is the angular velocity of the *EE*, the *EE* twist is $\mathbf{v} = [\dot{\mathbf{p}}^T \; \boldsymbol{\omega}^T]^T$ and its linear relationship with $\dot{\boldsymbol{\zeta}}$ is given by:

$$\mathbf{v} = \mathbf{D}(\boldsymbol{\epsilon})\dot{\boldsymbol{\zeta}}, \qquad \mathbf{D}(\epsilon) \overset{\Delta}{=} \begin{bmatrix} \mathbf{I}_{3\times3} & \mathbf{0}_{3\times3} \\ \mathbf{0}_{3\times3} & \mathbf{H}(\boldsymbol{\epsilon}) \end{bmatrix} \tag{2}$$

where $\mathbf{I}_{3\times3} \in \mathbb{R}^{3\times3}$ and $\mathbf{0}_{3\times3} \in \mathbb{R}^{3\times3}$ are identity and null matrices, and $\mathbf{H}(\boldsymbol{\epsilon})$ depends on the parametrization used to describe the orientation [2].

The rate of change of l_i, $\dot{l}_i$, can be computed as [3]:

$$\boldsymbol{\Xi}\mathbf{v} = \dot{\mathbf{l}}, \qquad \boldsymbol{\Xi} \overset{\Delta}{=} [\boldsymbol{\xi}_1 \cdots \boldsymbol{\xi}_n]^T, \qquad \dot{\mathbf{l}} \overset{\Delta}{=} [\dot{l}_1 \cdots \dot{l}_n]^T \tag{3}$$

where matrix $\boldsymbol{\Xi} \in \mathbb{R}^{n\times6}$ is the kinematic Jacobian of the manipulator, $\dot{\mathbf{l}}$ is the array stacking the time derivatives of the total cable lengths, and $\boldsymbol{\xi}_i$ is a zero-pitch screw directed as the cable-direction unit vector $\mathbf{t}_i$ (see Fig. 1), and passing through A_i:

$$\boldsymbol{\xi}_i = \begin{bmatrix} \mathbf{t}_i \\ \mathbf{a}'_i \times \mathbf{t}_i \end{bmatrix} \tag{4}$$

125 Generally $\mathrm{rank}(\boldsymbol{\Xi}) = n$, but it decreases in a direct-kinematics singularity [40].

If the lengths of the n cables are not varying in time, all kinematic constraints are active (that is, cables are taut), and $\boldsymbol{\Xi}$ has full column rank, the *EE* can still move on a variety of dimension $\lambda = 6 - n$ in SE(3), thus preserving λ *DoFs*. Consequently, λ components of $\boldsymbol{\zeta}$ are *free* to vary, and are called *free pose components* $\boldsymbol{\zeta}_f$. The remaining n components of $\boldsymbol{\zeta}$ are called 130 *dependent pose components* $\boldsymbol{\zeta}_d$, since they depend on the value of the fixed cable lengths $\mathbf{l}_0$ and free pose components $\boldsymbol{\zeta}_f$. In turn, this also means that the fixed cable lengths $\mathbf{l}_0$ are geometrical constant parameters when analyzing free-motion, and only need to be estimated once.

When actuators are locked, the *EE* motion is called *free motion*, and the *EE* kinematics can be described by setting $\dot{\mathbf{l}} = \mathbf{0}_{n\times1}$ in (3):

$$\boldsymbol{\Xi}\mathbf{v} = \mathbf{0}_{n\times1} \tag{5}$$

5

It was shown in [3] that the *free twist* $\mathbf{v}$, namely the expression of $\mathbf{v}$ that satisfies Eq. (5), can be expressed as a function of the *EE* λ residual *DoFs* as:

$$\mathbf{v} = \Xi^{\perp} \dot{\boldsymbol{\zeta}}_f \tag{6}$$

where $\Xi^{\perp}$ is a specific expression of the right nullspace of matrix Ξ: its derivation can be found in [3]. Consequently, the *EE* free-twist time derivative $\dot{\mathbf{v}}$ can be obtained by differentiating Eq. (6) w.r.t. time:

$$\dot{\mathbf{v}} = \Xi^{\perp} \ddot{\boldsymbol{\zeta}}_f + \dot{\Xi}^{\perp} \dot{\boldsymbol{\zeta}}_f \tag{7}$$

It should be noted that $\dot{\Xi}^{\perp}$, as any first-order time derivative, is linearly dependent on $\dot{\boldsymbol{\zeta}}_f$ and can be symbolically computed by differentiating the analytical expression of $\Xi^{\perp}$ w.r.t. time.

2.3. UACDPR Internal Dynamics

The non-linear dynamic model of an *UACDPR* emerges from the *EE* mechanical equilibrium, subject to cable constraints, inertial actions, and external wrenches [2]:

$$\mathbf{M}\dot{\mathbf{v}} + \mathbf{C}\mathbf{v} - \boldsymbol{\phi} = -\Xi^{T}\boldsymbol{\tau} \tag{8}$$

$$\mathbf{M} \triangleq \begin{bmatrix} m\mathbf{I}_{3\times3} & -m\tilde{\mathbf{s}}' \\ m\tilde{\mathbf{s}}' & \mathbf{I}_P \end{bmatrix}, \qquad \mathbf{C} \triangleq \begin{bmatrix} \mathbf{0}_{3\times3} & -m\tilde{\boldsymbol{\omega}}\tilde{\mathbf{s}}' \\ \mathbf{0}_{3\times3} & \tilde{\boldsymbol{\omega}}\mathbf{I}_P \end{bmatrix}, \qquad \boldsymbol{\phi} \triangleq m\begin{bmatrix} \mathbf{g} \\ \tilde{\mathbf{s}}'\mathbf{g} \end{bmatrix} \tag{9}$$

where m is the *EE* mass, $\mathbf{I}_P$ is the *EE* inertia matrix about its reference point P expressed in the inertial frame, the symbol $\sim$ over a vector denotes its skew-symmetric representation, and $\boldsymbol{\tau} \in \mathbb{R}^n$ is an array containing the cable-tension magnitudes. $\boldsymbol{\phi} \in \mathbb{R}^6$ is the external wrench due to gravity (Fig. 1), $\mathbf{s}'$ is the center of mass position w.r.t. P in the inertial frame, and $\mathbf{g}$ is the gravitational acceleration.

The *EE* internal dynamics, that is, the second-order nonholonomic constraint that the system variables must satisfy regardless of actuation and constraint actions [41], is obtained by pre-multiplying Eq. (8) by $\Xi^{\perp,T}$:

$$\Xi^{\perp,T}\left(\mathbf{M}\dot{\mathbf{v}} + \mathbf{C}\mathbf{v} - \boldsymbol{\phi}\right) = \mathbf{0}_{\lambda\times1} \tag{10}$$

3. Free Internal Dynamic Identification Model

In this Section, the linearity of *UACDPR* internal dynamics in the inertial parameters is outlined, and the *FIDIM* established. More specifically, it is shown that:

1. classical identification models may present difficulties in their application to *CDPRs*, because of the specific design of the actuators of this class of manipulators;

2. the internal dynamics of the *EE* can be used to derive a novel formulation of the identification problem, which is particularly suitable for *UACDPRs*;

3. the internal dynamics does not depend on the *EE* mass, but only on the *EE* center-of-mass location and its specific inertia tensor (that is, its inertia tensor divided by the *EE* mass), and it is linear in these parameters;

6

4. identification of the *EE* center-of-mass location and its specific inertia matrix can be performed without recurring to any force or torque measurement, since it only requires a direct measurement or estimation of λ *EE* coordinates, namely the free ones;

5. inertial parameters can be calculated as the *TLS* solution of an over-determined system of equations, obtained computing the internal dynamics over a sampled free-motion trajectory.

3.1. Computation of the identification model

Classical models for identification of *EE* inertial parameters aim at determining the *EE* mass, the *EE* center-of-mass position, and the *EE* inertia matrix components, which are the base parameters necessary to describe the *EE* dynamics [26]. To do so, *EE* dynamic equations are first rearranged, so that a linear equation in the inertial parameters is formulated. To this end, Eq. (8) may be rewritten as:

$$\begin{bmatrix} m(\ddot{\mathbf{p}} - \mathbf{g}) - m\tilde{\mathbf{s}}'\boldsymbol{\alpha} - m\tilde{\boldsymbol{\omega}}\tilde{\mathbf{s}}'\boldsymbol{\omega} \\ \mathbf{I}_P\boldsymbol{\alpha} + \tilde{\boldsymbol{\omega}}\mathbf{I}_P\boldsymbol{\omega} + m\tilde{\mathbf{s}}'(\ddot{\mathbf{p}} - \mathbf{g}) \end{bmatrix} = -\boldsymbol{\Xi}^T\boldsymbol{\tau} \tag{11}$$

The left-hand side of Eq. (11) can be algebraically manipulated in order to isolate the *EE* dynamic parameters. First, the vector product rule $\mathbf{a} \times \mathbf{b} = -\mathbf{b} \times \mathbf{a}$ is applied, so that:

$$\begin{bmatrix} m(\ddot{\mathbf{p}} - \mathbf{g}) + m(\tilde{\boldsymbol{\alpha}} + \tilde{\boldsymbol{\omega}}\tilde{\boldsymbol{\omega}})\mathbf{s}' \\ \mathbf{I}_P\boldsymbol{\alpha} + \tilde{\boldsymbol{\omega}}\mathbf{I}_P\boldsymbol{\omega} - m(\tilde{\ddot{\mathbf{p}}} - \tilde{\mathbf{g}})\mathbf{s}' \end{bmatrix} = -\boldsymbol{\Xi}^T\boldsymbol{\tau} \tag{12}$$

Then, we consider that $\mathbf{s}' \triangleq \mathbf{R}^P\mathbf{s}'$, and $\mathbf{I}_P \triangleq \mathbf{R}^P\mathbf{I}_P\mathbf{R}^T$, where $^P\mathbf{s}'$ and $^P\mathbf{I}_P$ are the (constant) center-of-mass coordinates and inertia tensor w.r.t. P expressed in the moving frame:

$$\begin{bmatrix} m(\ddot{\mathbf{p}} - \mathbf{g}) + m(\tilde{\boldsymbol{\alpha}} + \tilde{\boldsymbol{\omega}}\tilde{\boldsymbol{\omega}})\mathbf{R}^P\mathbf{s}' \\ \mathbf{R}^P\mathbf{I}_P\mathbf{R}^T\boldsymbol{\alpha} + \tilde{\boldsymbol{\omega}}\mathbf{R}^P\mathbf{I}_P\mathbf{R}^T\boldsymbol{\omega} - m(\tilde{\ddot{\mathbf{p}}} - \tilde{\mathbf{g}})\mathbf{R}^P\mathbf{s}' \end{bmatrix} = -\boldsymbol{\Xi}^T\boldsymbol{\tau} \tag{13}$$

If we consider the following identity in the product of a generic symmetric matrix $\mathbf{S}$ and a vector $\mathbf{v}$:

$$\mathbf{S}\mathbf{v} = \bar{\mathbf{v}}\check{\mathbf{S}} \tag{14}$$

where:

$$\mathbf{S} \triangleq \begin{bmatrix} S_{xx} & S_{xy} & S_{xz} \\ S_{xy} & S_{yy} & S_{yz} \\ S_{xz} & S_{yz} & S_{zz} \end{bmatrix} \qquad \mathbf{v} \triangleq \begin{bmatrix} v_x \\ v_y \\ v_z \end{bmatrix} \tag{15}$$

$$\bar{\mathbf{v}} \triangleq \begin{bmatrix} v_x & 0 & 0 & v_y & v_z & 0 \\ 0 & v_y & 0 & v_x & 0 & v_z \\ 0 & 0 & v_z & 0 & v_x & v_y \end{bmatrix} \qquad \check{\mathbf{S}} \triangleq \begin{bmatrix} S_{xx} & S_{yy} & S_{zz} & S_{xy} & S_{xz} & S_{yz} \end{bmatrix}^T \tag{16}$$

Equation (13) can be rewritten as:

$$\begin{bmatrix} m(\ddot{\mathbf{p}} - \mathbf{g}) + m(\tilde{\boldsymbol{\alpha}} + \tilde{\boldsymbol{\omega}}\tilde{\boldsymbol{\omega}})\mathbf{R}^P\mathbf{s}' \\ (\overline{\mathbf{R}^P\boldsymbol{\alpha}} + \tilde{\boldsymbol{\omega}}\overline{\mathbf{R}^P\boldsymbol{\omega}})^P\check{\mathbf{I}}_P - m(\tilde{\ddot{\mathbf{p}}} - \tilde{\mathbf{g}})\mathbf{R}^P\mathbf{s}' \end{bmatrix} = -\boldsymbol{\Xi}^T\boldsymbol{\tau} \tag{17}$$

where $^P\boldsymbol{\alpha} = \mathbf{R}^T\boldsymbol{\alpha}$ and $^P\boldsymbol{\omega} = \mathbf{R}^T\boldsymbol{\omega}$ are the angular acceleration and velocity vectors expressed in the moving frame.

7

Finally, the *EE* dynamics can be expressed as a linear equation in the *EE* inertial parameters m, $m^P\mathbf{s}\prime$, and $^P\breve{\mathbf{I}}_P$ as:

$$\mathbf{W}_{EE}(\boldsymbol{\zeta},\dot{\boldsymbol{\zeta}},\ddot{\boldsymbol{\zeta}})\boldsymbol{\chi}_{EE} = -\Xi^T(\boldsymbol{\zeta})\boldsymbol{\tau} \tag{18}$$

where:

$$\mathbf{W}_{EE} \triangleq \begin{bmatrix} (\ddot{\mathbf{p}} - \mathbf{g}) & (\tilde{\boldsymbol{\alpha}} + \tilde{\boldsymbol{\omega}}\tilde{\boldsymbol{\omega}})\mathbf{R} & \mathbf{0}_{3\times 6} \\ \mathbf{0}_{3\times 1} & -(\check{\ddot{\mathbf{p}}} - \check{\mathbf{g}})\mathbf{R} & (\mathbf{R}\overline{^P\boldsymbol{\alpha}} + \tilde{\boldsymbol{\omega}}\mathbf{R}\overline{^P\boldsymbol{\omega}}) \end{bmatrix}, \qquad \boldsymbol{\chi}_{EE} \triangleq \begin{bmatrix} m \\ m^P\mathbf{s}\prime \\ ^P\breve{\mathbf{I}}_P \end{bmatrix} \tag{19}$$

with $\mathbf{W}_{EE} \in \mathbb{R}^{6\times 10}$, and $\boldsymbol{\chi}_{EE} \in \mathbb{R}^{10\times 1}$.

The application of Eq. (18) over a trajectory which is sampled in n_s configurations leads to defining an over-determined system of $6n_s$ equations in 10 unknowns, which can be solved for $\boldsymbol{\chi}_{EE}$ and analyzed with the tools of linear regression. To this end, the elements of $\mathbf{W}_{EE}$, Ξ, and $\boldsymbol{\tau}$ need to be computed at all trajectory time instants. The *EE* motion can be measured, for example by means of an external photogrammetry system or a laser tracker, or estimated by means of direct kinematics or inertial measurement units. Cable tensions can be measured by means of force sensors embedded in the cable transmission [29], or estimated by modelling its actuation unit [28]. It should be noted that, in general, the *UACDPR EE* pose and its derivatives cannot be inferred by means of direct kinematics only, and additional sensors must be employed if a pose measuring device is to be avoided. As an example, encoders on swivel axes could be employed [19], but their efficacy for pose reconstruction has not been tested in dynamical applications.

Even though identification through Eq. (18) is theoretically feasible, there are two main drawbacks in its use:

- force sensors need to be embedded in the cable transmission (either at the cable attachment points on the platform, or within the swivel-pulley system [42]), which complicates the mechatronic design of the robot and increases its cost; in addition, force sensors may not be particularly accurate in predicting cable tensions, since their readings may be disturbed by several factors, the most important of which is friction in the cable transmission;

- common winch designs [42, 43] include multiple rototranslating elements, which represent severe sources of friction: high friction is a serious problem for identification, because of its unpredictable nature; the transition between static and kinematic friction adds high-frequency effects to motor current signals, which needs to be carefully filtered before being used for estimating cable tensions.

Ultimately, directly measuring cable tensions, or estimating them via winch modeling, may lead to low cable-tension accuracy, which in turn would negatively impact the overall identification process.

Thus, an alternative formulation of the identification model is here proposed, which aims at determining *EE* inertial parameters, without measuring or estimating cable tensions. We start by observing that if Eq. (18) is pre-multiplied by $\Xi^{\perp^T}$, the right-hand side of Eq. (18) vanishes:

$$\Xi^{\perp^T}\mathbf{W}_{EE}\boldsymbol{\chi}_{EE} = \mathbf{0}_{\lambda\times 1} \tag{20}$$

Scalar identification relations in Eq. (20) are fewer than in Eq. (18), namely λ instead of n, so that the identification trajectory must be sampled in more points $n_s' > n_s$, but no force or

torque measurement is now needed: the computation of $\Xi^{\perp}$ and $\mathbf{W}_{EE}$ in Eq. (20) only requires the *EE* pose to be measured, and its numerical differentiation. In addition, since the internal dynamics is linear in $\boldsymbol{\chi}_{EE}$ and homogeneous, its validity is not impacted by the multiplication or division by a non-zero scalar. Thus, we can deduce that the *EE* internal dynamics is not influenced by the *EE* mass, and we can divide Eq. (20) by m:

$$\mathbf{W}'_{EE}\boldsymbol{\chi}'_{EE} = \mathbf{0}_{\lambda \times 1} \tag{21}$$

where:

$$\mathbf{W}'_{EE} \overset{\Delta}{=} \Xi^{\perp T}\mathbf{W}_{EE}, \qquad \boldsymbol{\chi}'_{EE} \overset{\Delta}{=} \begin{bmatrix} 1 \\ {}^{P}\mathbf{s}' \\ {}^{P}\check{\mathbf{I}}'_{P} \end{bmatrix}, \qquad {}^{P}\check{\mathbf{I}}'_{P} \overset{\Delta}{=} {}^{P}\check{\mathbf{I}}_{P}/m \tag{22}$$

It should be noted that in case the *EE* mass needs to be identified, it can be inferred by detaching the *EE* and by weighting it. In case the detachment of the platform is not possible, an alternative solution can be adding a known payload of mass Δm to the *EE* in a known location (${}^{P}\mathbf{p}'_{L}$ is the position vector of the payload center of mass in the moving frame) and identify the new *EE* with the additional payload [44]. If the total center of mass of the *EE* with the additional payload is denoted by ${}^{P}\mathbf{s}'_{L}$, the definition of center of mass gives:

$$(m + \Delta m){}^{P}\mathbf{s}'_{L} = m{}^{P}\mathbf{s}' + \Delta m{}^{P}\mathbf{p}'_{L} \tag{23}$$

and the *EE* mass m can be determined from:

$$m({}^{P}\mathbf{s}'_{L} - {}^{P}\mathbf{s}') = \Delta m({}^{P}\mathbf{p}'_{L} - {}^{P}\mathbf{s}'_{L}) \tag{24}$$

190   The knowledge of the standard deviations associated with the identified values of ${}^{P}\mathbf{s}'_{L}$ and ${}^{P}\mathbf{s}'$ may provide a weighting strategy for the solution of the over-determined system of equations given in Eq. (24).

Equation (21) is valid in general for *UACDPRs*, but it can be further specialized in order to simplify experimental identification. In fact, *in case the EE exciting trajectory is a free-motion* 195 *one*, the expression of $\boldsymbol{\zeta}$ and its derivatives, which are needed to compute the elements of $\mathbf{W}'_{EE}$, depends only on the *constant* value of the cable lengths, $\mathbf{l}_0$, and on the λ free coordinates of the *EE* $\boldsymbol{\zeta}_f$ (and its derivatives).

3.2. Total-Least-Square Identification

Equation (21) is applied to n'_s configurations deriving from one or more free-motion trajectories, thus establishing the *FIDIM*. Usually, the n'_s samples are obtained by over-sampling the *EE* free coordinates at high frequency, then by band-pass filtering them, and finally by decimating them [45]. This results in the over-determined system of equations:

$$\mathbf{W}\boldsymbol{\chi} = \mathbf{0}_{\lambda n'_s \times 1}, \qquad \mathbf{W} = \begin{bmatrix} \mathbf{W}'_{EE,1} \\ \vdots \\ \mathbf{W}'_{EE,n'_s} \end{bmatrix} \tag{25}$$

where matrix $\mathbf{W} \in \mathbb{R}^{\lambda n'_s \times 10}$ is called *regressor* or *identification* matrix and vector $\boldsymbol{\chi} = \boldsymbol{\chi}'_{EE} \in \mathbb{R}^{10 \times 1}$ comprise the *EE base inertial parameters*, that is, the minimal set of independent parameters necessary to describe the *EE* dynamics [26]. Ideally, rank($\mathbf{W}$) = 9, and infinite solutions of Eq. (25) can be found. On the other hand, there are two primary sources of errors which are not considered in Eq. (25), so that in practice rank($\mathbf{W}$) = 10: measurement

9

errors, and also model errors. The former errors, which depend on the measurement equipment and/or the estimation methodology used to compute ζ_f, may be amplified due to the numerical differentiation needed to obtain $\dot{\zeta}_f$ and $\ddot{\zeta}_f$, and the strong dependence on kinematic parameters, since matrices $\Xi^\perp$ and $\dot{\Xi}^\perp$ are employed both for internal dynamics (c.f. Eq. (22)) and the computation of the free twist and its derivative (c.f. Eqs. (6),(7)). As a consequence, matrix $\mathbf{W}$ can be more realistically modelled as $\mathbf{W} + \Delta\mathbf{W}$. Model errors are accounted for by considering that the right-hand side of Eq. (25) is not a zero vector, but an error vector $\boldsymbol{\varepsilon} \in \mathbb{R}^{\lambda n'_s \times 1}$:

$$(\mathbf{W} + \Delta\mathbf{W})\boldsymbol{\chi} = \boldsymbol{\varepsilon} \tag{26}$$

The *TLS* solution of Eq. (26) is therefore considered. This technique allows $\boldsymbol{\chi}$ to be computed while minimizing both $\Delta\mathbf{W}$ and $\boldsymbol{\varepsilon}$ [38], as opposed to Least-Square and Output-Error methods, that would only minimize $\boldsymbol{\varepsilon}$. According to the *TLS* technique, the real system $(\mathbf{W} + \Delta\mathbf{W})\boldsymbol{\chi} = \boldsymbol{\varepsilon}$ is changed to its closest compatible system of the form:

$$\hat{\mathbf{W}}\hat{\boldsymbol{\chi}} = \mathbf{0}_{\lambda n'_s \times 1} \tag{27}$$

where $\text{rank}(\hat{\mathbf{W}}) = 9 < 10 = \text{rank}(\mathbf{W})$, and $\hat{\mathbf{W}}$ is closest to $\mathbf{W}$ with respect to the Frobenius norm, i.e. $\hat{\mathbf{W}}$ minimizes the Frobenius norm $\|\hat{\mathbf{W}} - \mathbf{W}\|_F$. Accordingly, $\hat{\boldsymbol{\chi}}$ is the solution of Eq. (27) and the *TLS* solution of Eq. (26).

$\hat{\mathbf{W}}$ can be straightforwardly computed by performing the *Singular Value Decomposition (SVD)* of $\mathbf{W}$:

$$\mathbf{W} = \mathbf{U} \begin{bmatrix} \mathbf{S} \\ \mathbf{0}_{(\lambda n'_s - 10) \times 10} \end{bmatrix} \mathbf{V}^T \tag{28}$$

where $\mathbf{U}$ and $\mathbf{V}$ are, respectively, $(\lambda n'_s \times \lambda n'_s)$ and (10×10) orthonormal matrices, and $\mathbf{S}$ is the (10×10) diagonal matrices of $\mathbf{W}$ singular values (which we assume to be sorted in decreasing order). Then, $\hat{\mathbf{W}}$ is calculated as [38]:

$$\hat{\mathbf{W}} = \mathbf{W} - s_{10}\mathbf{U}_{10}\mathbf{V}_{10}^T \tag{29}$$

where s_{10} is the smallest singular value of $\mathbf{W}$, and $\mathbf{U}_{10}$ and $\mathbf{V}_{10}^T$ are the *10*-th columns of $\mathbf{U}$ and $\mathbf{V}^T$, respectively. Then, the *TLS* solution of Eq. (25) is given by:

$$\boldsymbol{\chi} = \mathbf{V}_{10} \tag{30}$$

where $\boldsymbol{\chi}$ is normalized so as to have 1 in its first element, according to the second definition in Eq. (22).

Standard deviations σ_{χ_i}, with $i = 2,\ldots,10$, on the dynamic parameters are estimated assuming that errors in the identification matrix $\mathbf{W}$ are independent and identically distributed with zero mean and common covariance σ_W^2 [35]. An unbiased estimator of the standard deviation σ_W is given by [38]:

$$\sigma_W = \frac{s_{10}}{\sqrt{\lambda n'_s - 10}} \tag{31}$$

and the covariance matrix of the *TLS* solution error is approximated by:

$$\mathbf{C}_\chi = \sigma_W^2 \left(1 + \|\boldsymbol{\chi}_{2:10}\|_2^2\right) \left(\hat{\mathbf{W}}_{2:10}^T \hat{\mathbf{W}}_{2:10}\right)^{-1} \tag{32}$$

10

where $\boldsymbol{\chi}_{2:10}$ contains every element of $\boldsymbol{\chi}$ except the first one, and $\hat{\mathbf{W}}_{2:10}$ contains all columns of $\hat{\mathbf{W}}$ except the first one. Finally, standard deviations on the inertial parameters are given by:

$$\sigma_{\chi_i} = \sqrt{\mathbf{C}_\chi(i,i)}, \qquad i = 2,\ldots,10 \tag{33}$$

where $\mathbf{C}_\chi(i,i)$ is the i-th diagonal term of $\mathbf{C}_\chi$, and its relative value with respect to the identified parameter is:

$$\sigma_{\%\chi_i} = 100\sigma_{\chi_i}/\|\chi_i\| \tag{34}$$

If the value of $\sigma_{\%X_i}$ is lower than 10%, the corresponding parameter is commonly consid-
ered to be well-identified [46]. There are mainly 2 scenarios in which the values of $\sigma_{\%\chi_i}$ may
be large, which require different additional steps:

- in case the parameter χ_i is near zero, $\sigma_{\%\chi_i}$ may naturally be very large: this kind of pa-
  rameters are called *non-essentials* [46] and can be removed from the dynamic model,
  because their influence is very limited; by removing them from vector $\boldsymbol{\chi}$ and the corre-
  sponding column from matrix $\mathbf{W}$, the *TLS* analysis can be re-performed with possibly
  higher-accuracy results;

- in case the parameter χ_i is not near zero, it means that something went wrong during
  experiments, or the parameters to be estimated are not the base ones: in the former
  case, the possible causes are, for examples, inadequate measurement systems, estima-
  tion procedures, or excitation trajectories, and experiments should be re-performed,
  whereas the latter case requires the dynamic model to be reduced so that it explicitly
  depends on base parameters only [26].

4. Optimal Free-Motion Excitation

The identification procedure requires the robot *EE* to perform a trajectory, so that *EE* co-
ordinates can be sampled and the regressor matrix $\mathbf{W}$ computed. The problem of generating
optimal exciting motion was extensively studied in the literature [47]. Optimal exciting trajec-
tories commonly aim at *determining robot actuator motion laws* by the *constrained non-linear
optimization of some cost function* correlated with the identification problem [48]. Thus, ex-
periment design focuses on two aspects: how to excite the system, and what to optimize.

Actuator motion laws may be parametric polynomials [47], B-splines [49], sinusoidal [50]
or other functions, so that the parameters upon which they depend can be determined as the
solution of the optimal excitation problem. Depending on the manipulator under study, the
choice of a type of trajectory may have specific advantages. For example, if the joints of a
serial manipulator are excited by sinusoidal motion laws, small control errors on joint angles
may introduce noise in joint speed and acceleration. Since the nominal trajectory is periodic
and band-limited, it is quite easy to design a post-processing filter aiming at removing unde-
sired noise from speed and acceleration signals, which are needed for identification [50]. In
our case, we chose to apply the exciting motion not to actuators, but to free-coordinates: the
optimal identification results reported in [31] demonstrated this approach to be both feasible
and effective for systems similar to *UACDPRs*. This motion is naturally sinusoidal *if the oscilla-
tion amplitude is limited*. Indeed, [3] analyzed small-amplitude free motions of the *EE* about
equilibrium configurations, and experimentally verified that its sinusoidal approximation is

11

true in practice. Thus, the *EE* small-amplitude free motion has the same benefits as actuator sinusoidal excitation, i.e. ease of filtering, and can beneficially be chosen as an exciting trajectory.

In the following, *EE* small-amplitude free motion is characterized in more detail, in order to determine which excitation parameters need to be optimized. If the expression of the free twist $\mathbf{v}$ and its derivative $\dot{\mathbf{v}}$ given in Eqs. (6) and (7) are substituted in Eq. (10), the free-motion internal dynamics can be written as [3]:

$$\mathbf{M}^{\perp}\ddot{\boldsymbol{\zeta}}_f + \mathbf{C}^{\perp}\dot{\boldsymbol{\zeta}}_f - \boldsymbol{\phi}^{\perp} = \mathbf{0}_{\lambda \times 1} \tag{35}$$

where:

$$\mathbf{M}^{\perp} \overset{\Delta}{=} \boldsymbol{\Xi}^{\perp T}\mathbf{M}\boldsymbol{\Xi}^{\perp}, \qquad \mathbf{C}^{\perp} \overset{\Delta}{=} \boldsymbol{\Xi}^{\perp T}\left(\mathbf{M}\dot{\boldsymbol{\Xi}}^{\perp} + \mathbf{C}\boldsymbol{\Xi}^{\perp}\right), \qquad \boldsymbol{\phi}^{\perp} \overset{\Delta}{=} \boldsymbol{\Xi}^{\perp T}\boldsymbol{\phi} \tag{36}$$

Equation (35) can be linearized about an equilibrium value of $\boldsymbol{\zeta}_f$, namely $\boldsymbol{\zeta}_{f0}$, that depends on the value of the constant cable lengths $\mathbf{l}_0$, resulting in:

$$\mathbf{M}_0^{\perp}\Delta\ddot{\boldsymbol{\zeta}}_{f0} + \mathbf{K}_0^{\perp}\Delta\boldsymbol{\zeta}_{f0} = \mathbf{0}_{\lambda \times 1} \tag{37}$$

where $\Delta\ddot{\boldsymbol{\zeta}}_{f0} \overset{\Delta}{=} \ddot{\boldsymbol{\zeta}}_f - \mathbf{0}_{\lambda \times 1}$ and $\Delta\boldsymbol{\zeta}_{f0} \overset{\Delta}{=} \boldsymbol{\zeta}_f - \boldsymbol{\zeta}_{f0}$. $\mathbf{M}_0^{\perp}$ is given in Eq. (36) and calculated in the equilibrium configuration, whereas $\mathbf{K}_0^{\perp}$ is known as the *Free-Motion Stiffness*, and its formulation can be found in [3].

By considering a solution of Eq. (37) in the form:

$$\Delta\boldsymbol{\zeta}_{f0}(t) = \sum_{j=1}^{\lambda} \Delta\boldsymbol{\zeta}_{f0,j}(t) \tag{38}$$

$$\Delta\boldsymbol{\zeta}_{f0,j}(t) = A_j\boldsymbol{\gamma}_j \cos\left(2\pi f_j t - \varphi_j\right) \tag{39}$$

we may conclude that the free-motion excitation is influenced, for each mode of oscillation $j = 1, \ldots, \lambda$, by oscillation amplitude A_j, eigenvector $\boldsymbol{\gamma}_j$, frequency f_j and phase φ_j. On the other hand, these parameters cannot be physically selected during an experiment, since they depend on other physical quantities, which are to be optimized on their behalf. More specifically, these parameters depend on:

- *UACDPR* cable lengths, whose fixed values allow for the determination of the equilibrium configuration, and thus for the computation of $\boldsymbol{\gamma}_j$ and f_j;

- initial displacement and velocity of the free coordinates, which are the initial conditions of the free-motion internal dynamics, and allow A_j and φ_j to be computed.

The total number of parameters to be determined is thus $n + 2\lambda$, that is, n cable lengths $\mathbf{l}_0$ and 2λ free-motion initial conditions $\Delta\boldsymbol{\zeta}_{f0}(0)$ and $\Delta\dot{\boldsymbol{\zeta}}_{f0}(0)$. In order to simplify the experiment design, $\Delta\dot{\boldsymbol{\zeta}}_{f0}(0)$ can be chosen to be the zero vector[3], which means to assign a zero initial velocity to the *EE* free-motion. Accordingly, the *EE* should be displaced w.r.t. its equilibrium configuration, kept still to make its velocity vanish, and then left to oscillate. It should be noted that the oscillation about a single equilibrium configuration is unlikely to result in a satisfactory

---

[3]This implies $\varphi_j = 0$, for every j.

identification, since the resulting identification matrix would be biased: therefore, a better option is to let *EE* oscillate about n_e different equilibria, so that the optimal excitation algorithm should determine $\mathbf{l}_{0,k}$ and $\Delta\boldsymbol{\zeta}_{f0,k}(0)$ ($k = 1,\dots,n_e$), for a total of $n_e(n+\lambda)$ parameters. Note that, in case an equal number of samples per equilibria n_s^e is chosen, the total number of samples per identification would be $n_s' = n_s^e n_e$.

The cost function to be minimized in order to determine optimal excitation parameters is always correlated to two main factors:

- the elements of the covariance matrix in Eq. (32) should be small: the smaller its elements, the higher the accuracy of the identification [51];

- the numerical solution of the identification problem, that is, the SVD decomposition of $\mathbf{W}$, should be stable: slight changes in the excitation trajectory should not negatively affect the identification-problem solution [52].

Practically, both of these issues are tackled by minimizing:

$$C = \frac{s_1}{s_9} + \frac{1}{s_9} = \frac{s_1 + 1}{s_9} \tag{40}$$

Since s_1 and s_9 are the largest and the smallest non-zero singular value of $\hat{\mathbf{W}}$, minimizing s_1/s_9 amounts to requiring that the condition number of $\hat{\mathbf{W}}$ is minimum[4]. Since the aforementioned ratio could be minimum for small or large singular values alike, the additional minimization of $1/s_9$ amounts to requiring the singular values to be as large as possible. In fact, the magnitude of the elements of matrix $\left(\hat{\mathbf{W}}_{2:10}^T \hat{\mathbf{W}}_{2:10}\right)^{-1}$ depends on the inverse of the singular values [52]. Thus, we propose the non-linear optimization problem:

$$\left[\mathbf{l}_{0,1},\dots,\mathbf{l}_{0,n_e},\Delta\boldsymbol{\zeta}_{f0,1}(0),\dots,\Delta\boldsymbol{\zeta}_{f0,n_e}(0)\right] = \text{argmin}\,(C) \tag{41}$$

subject to:

$$\begin{cases} \tau_i(t) \leq \tau_M, & \forall i, t \\ \tau_i(t) \geq \tau_m, & \forall i, t \\ -\Delta\boldsymbol{\zeta}_{fL} \leq \Delta\boldsymbol{\zeta}_{f0}(t) \leq \Delta\boldsymbol{\zeta}_{fL}, & \forall t \end{cases} \tag{42}$$

where τ_i is the i-th cable tension, τ_m and τ_M are minimum and maximum cable tension limits, and $\Delta\boldsymbol{\zeta}_{fL}$ is an upper limit for the oscillation of the free coordinates. These constraints essentially require the trajectory to be (dynamically) wrench-feasible and oscillations to have a limited amplitude. The theoretical absolute minimum value of the cost function is 1: this information is useful because it allows us to determine how close a real experiment is to theoretical optimality. In practice, a value of $C < 100$ is typically considered good, whereas $C < 10$ is optimal [47, 54].
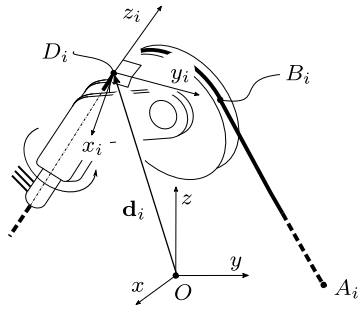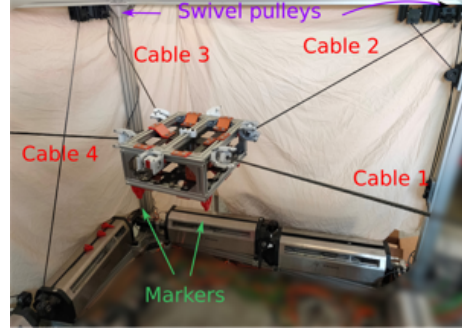
5. Experimentation

In this Section, the optimal free-motion excitations of a 4-cable *UACDPR* are computed according to the results of Section 4, and its inertial parameters are determined according

---

[4]Note that the minimum value of the condition number is 1[53]

13

(a) *Swivel pulley local view*　　　　　　　　(b) UACDPR *Prototype*

Figure 2: CDPR *geometric model*

Table 1: Actuators' properties

i	1	2	3	4
$\mathbf{d}_i$ [m]	$\begin{bmatrix} 0.219 \\ -1.316 \\ 0.527 \end{bmatrix}$	$\begin{bmatrix} 2.295 \\ -1.158 \\ 0.521 \end{bmatrix}$	$\begin{bmatrix} 2.153 \\ 0.973 \\ 0.560 \end{bmatrix}$	$\begin{bmatrix} 0.0532 \\ 0.796 \\ 0.532 \end{bmatrix}$
r_i [m]	0.025	0.025	0.025	0.025
$^P\mathbf{a}'_i$ [m]	$\begin{bmatrix} -0.144 \\ -0.219 \\ 0.264 \end{bmatrix}$	$\begin{bmatrix} 0.115 \\ -0.233 \\ 0.270 \end{bmatrix}$	$\begin{bmatrix} 0.142 \\ 0.220 \\ 0.266 \end{bmatrix}$	$\begin{bmatrix} -0.120 \\ 0.236 \\ 0.266 \end{bmatrix}$
$\mathbf{x}_i$	$\mathbf{j}$	$-\mathbf{i}$	$-\mathbf{j}$	$\mathbf{i}$
$\mathbf{y}_i$	$-\mathbf{k}$	$-\mathbf{k}$	$-\mathbf{k}$	$-\mathbf{k}$
$\mathbf{z}_i$	$-\mathbf{i}$	$-\mathbf{j}$	$\mathbf{i}$	$\mathbf{j}$

to *FIDIM*, as proposed in Section 3. The geometrical properties of the prototype used for experimentations (Fig. 2b) are summarized in Table 1, where $\mathbf{i} = [1;0;0]^T$, $\mathbf{j} = [0;1;0]^T$, and $\mathbf{k} = [0;0;1]^T$. The coordinates of $\mathbf{a}'_i$ are constant in the *EE* frame, and denoted as $^P\mathbf{a}'_i$. Since the prototype is equipped with swivel pulleys, their kinematic model parameters (see Fig. 2a) are also reported in table 1: r_i is the pulley radius, $\mathbf{d}_i$ is the position of D_i, $\mathbf{z}_i$ is the direction of the swivel axis, $\mathbf{x}_i$ and $\mathbf{y}_i$ are fixed unit vectors perpendicular to $\mathbf{z}_i$.

5.1. Optimal Excitation Computation

The x and y coordinates of the *EE* reference point were chosen as *UACDPR* free coordinates. This choice aims at minimizing experimental effort, thus cost and complexity: these coordinates are straightforwardly recorded by an external measurement system, if a marker is placed on the reference point. Orientation measurements would require additional markers mounted on the platform and a mathematical model aiming at extracting orientation information from the relative position of points. Tension and oscillation limits were set to

14

Table 2: Optimized cable lengths (in [m])

k	1	2	3	4	5	6	7	8	9	10	11	12
l_1	1.66	1.32	1.30	1.52	1.11	1.38	1.19	1.16	1.46	1.43	1.35	1.52
l_2	1.86	1.58	1.26	1.26	1.68	1.39	1.15	1.17	1.16	1.37	1.45	1.12
l_3	1.68	1.99	1.57	1.27	2.19	1.36	1.65	1.63	1.24	1.27	1.42	1.17
l_4	1.41	1.76	1.56	1.50	1.72	1.32	1.65	1.59	1.50	1.30	1.28	1.54

Table 3: Optimized free coordinate displacements $\Delta\boldsymbol{\zeta}_{f0}(0)$ (in [mm])

k	1	2	3	4	5	6	7	8	9	10	11	12
x	5.01	4.34	39.3	76.0	4.22	25.3	1.97	24.9	43.8	47.0	2.37	96.9
y	2.21	7.11	17.6	14.4	7.95	16.6	10.9	9.70	17.4	1.51	11.7	99.7

$\tau_m = 20\text{N}$, $\tau_M = 200\text{N}$ and $\Delta\boldsymbol{\zeta}_{fL} = [0.1, 0.1]^T$ m. The trajectory optimization problem in Eq. (41) was solved considering nominal dynamic parameters estimated by *CAD*:

$$
{}^{P}\mathbf{s}_l = \begin{bmatrix} 0 \\ 0 \\ 0.19 \end{bmatrix} \text{m}, \qquad {}^{P}\breve{\mathbf{I}}'_P = \begin{bmatrix} 0.051 \\ 0.069 \\ 0.037 \\ 0 \\ 0 \\ 0 \end{bmatrix} \text{Kg}\cdot\text{m}^2 \tag{43}
$$

Since Eq.(41) is nonlinear and its gradient is not readily available, it was numerically solved by using *fmincon* MATLAB function, which employs an interior-point algorithm [39] and nu-
290 merically estimates cost function gradient. Additionally, a *multistart* algorithm was employed in order to automatically provide 100 randomly selected initial guesses for $\mathbf{l}_{0,k}$ and $\Delta\boldsymbol{\zeta}_{f0,k}(0)$, with $k = 1, \dots, n_e$. Note that the numerical solution of the optimization problem requires also to chose the number of equilibrium configuration, n_e, and the number of samples per equilibrium, n_s^e. They were tuned to $n_e = 12$ and $n_s^e = 100$ for optimal results, as discussed below.
295 The cost function was optimized[5] to $C = 5.94$, resulting in cable lengths as in Tab. 2 and free-coordinate displacements as in Tab. 3. This result is very good w.r.t. identification best practices [47, 54], thus different, and possibly more efficient, optimization techniques were not explored.

It should be noted that the multistart algorithm provided a large number of local min-
300 ima with a cost function value $C < 10$ (the multistart optimization was run several times for robustness, with negligible variations in results), showing that:

- optimization results are very limitedly influenced by the choice of equilibria upon which the *EE* oscillates: every time the optimization was solved, different optimal values for cable lengths and initial free coordinate displacements were found, most of which re-
305 sulted in a cost function value $C < 10$;

---

[5]Average computation time for each optimization performed by the multistart algorithm is 36s, on a personal computer with an Intel I7 8th generation processor, and 16 Gb of RAM.

- the different equilibrium configurations about which the platform oscillates are randomly positioned in the robot wrench-feasible reachable workspace: this fact is probably related to a low bias typically induced by randomness;

- minimal values of C are found for large free-coordinate oscillations: their maximum values are such that cable tension values meet their limits for some t.

Therefore, randomly selecting *UACDPR* equilibrium configurations and letting the platform oscillate without cables losing tension might provide optimal identification results, since the values of parameters resulting in a cost function $C < 10$ are equally optimal in practice. It should be noted that this conclusion is true for the robot considered in this paper, but it may not be so in other cases, mainly if special geometrical and/or inertial parameters are used.

On the other hand, the number of different equilibria n_e upon which the *EE* should oscillate, and the number of samples per equilibria n_s^e, appear to have a far larger influence on the cost-function minimal value. Simulations showed that a number of equilibria between 8 and 16, and a number of samples per equilibria n_s^e between 50 and 150, performed satisfactorily, resulting in $C < 50$. $n_e = 12$ and $n_s^e = 100$ were thus chosen because they provided $C < 10$ most of the times. It is worth observing that, depending on the measurement system employed to estimate the *EE* free coordinates $\boldsymbol{\zeta}_f$, the estimation-model sensitivity to measurement errors could impact the cost-function minimal value, as well as identification overall results.

5.2. Identification results

Based on the results of optimal free-motion excitation, experimental analysis was conducted on randomly selected configurations. In order to acquire the data necessary for identification purpose:

- the platform was brought to 12 random locations, different from the ones determined in Sec. 5.1 (and reported in Tab. 3), inside the robot wrench-feasible reachable workspace;

- the cables were commanded to hold their lengths (i.e. the motors were commanded to hold their angular position); encoder angular positions were recorded so as to determine the experimental value of the cable lengths $\mathbf{l}_0^\star$;

- cable tensions were checked to be positive, based on motor current readings;

- the platform was manually slightly displaced from the equilibria by an operator, by holding the platform by hand;

- operator hands were moved away from the platform, so that the latter could freely oscillate.

An automatic excitation strategy will be sought in the future, since this manual excitation procedure is far from being practical or ideal, but it is sufficient for the demonstration of the proposed identification technique.

The position of the optical marker placed onto the *EE* reference point was tracked by 8 cameras of a VICON Motion Capture System[6] (measurement accuracy was ±0.2 mm for each

---

[6]As an alternative to optical measurements, if the robot design allows it, *EE* free coordinates may be estimated by means of cable angle measurements and direct kinematics, as proposed in [55], and applied in [31], or by means of Inertial Measurement Units [29].

marker's Cartesian component, at a 100 Hz sampling rate) for a total duration of 10 s for each experiment, thus acquiring 1001 samples per marker coordinate[7]. The initial values of marker positions before oscillations were regarded as the equilibrium position of the *EE*.

These recorded coordinates were then filtered by using a zero-phase finite-impulse response low-pass digital filter with a stop-band frequency of 10 Hz. Then, signals were numerically differentiated in order to obtain the linear velocity and acceleration of the reference point, and ultimately decimated in order to obtain 100 samples per experiment. The total number of samples was thus $n'_s = 1200$.

The x and y coordinates of the marker were selected as *EE* free coordinates $\boldsymbol{\zeta}_f$. Accordingly, the experimental value of the controlled coordinates $\boldsymbol{\zeta}_c^\star$ were determined, for all t, as the numerical solution of the non-linear problem defined by:

$$\begin{cases} l_1(\boldsymbol{\zeta}_f^\star, \boldsymbol{\zeta}_c) - l_{1,0}^\star = 0 \\ \vdots \\ l_n(\boldsymbol{\zeta}_f^\star, \boldsymbol{\zeta}_c) - l_{n,0}^\star = 0 \end{cases} \tag{44}$$

where $l_i(\boldsymbol{\zeta}_f, \boldsymbol{\zeta}_c)$ is calculated as in Eq. (1), $\boldsymbol{\zeta}_f^\star$ contains the measured free coordinates, and $l_{i,0}^\star$ is the measured i-th cable length. Then, the *EE* twist and its time derivative were determined as (cf. Eqs. (6) and (7)):

$$\mathbf{v} = \boldsymbol{\Xi}_l^\perp \dot{\boldsymbol{\zeta}}_f, \qquad \dot{\mathbf{v}} = \dot{\boldsymbol{\Xi}}_l^\perp \dot{\boldsymbol{\zeta}}_f + \boldsymbol{\Xi}_l^\perp \ddot{\boldsymbol{\zeta}}_f \tag{45}$$

Finally, by collecting all experiment data, the *TLS* solution of the identification problem in Eq. (25), $\boldsymbol{\chi}_{free}$, was obtained as:

$$\boldsymbol{\chi}_{free} = \begin{bmatrix} 1 \\ {}^P\mathbf{s}\prime \\ {}^P\breve{\mathbf{I}}_P' \end{bmatrix} = \begin{bmatrix} 1 \\ 0.002 \\ -0.0025 \\ 0.1984 \\ 0.0569 \\ 0.0627 \\ 0.0314 \\ 2e-4 \\ -2e-4 \\ 1.6e-4 \end{bmatrix}, \qquad \boldsymbol{\sigma}_{\%\chi,free} = \begin{bmatrix} 0 \\ 4.32 \\ 3.09 \\ 0.15 \\ 0.64 \\ 0.31 \\ 1.76 \\ 80.5 \\ 99.4 \\ 136 \end{bmatrix}, \qquad \sigma_W = 0.536, \qquad C = 8.36 \tag{46}$$

Additional experiments were conducted by measuring the full *EE* pose during free motion, by means of additional markers mounted onto the platform. Thus, the use of Eqs. (44) and (45) was avoided, since pose data were complete, and the *EE* twist and its derivatives could be obtained by numerically differentiating the pose. The *TLS* solution of the identification

---

[7]The recording of the optical marker position starts a while after the operator hands are moved away from the platform, when the end-effector oscillates with small amplitude about its equilibrium configuration, so that cable tensions also oscillates about their positive equilibrium value.

problem in Eq. (25) corresponding to these data was obtained as:

$$\boldsymbol{\chi}_{full} = \begin{bmatrix} 1 \\ 0.0016 \\ -0.0025 \\ 0.2 \\ 0.0563 \\ 0.0627 \\ 0.0322 \\ 4.8e-5 \\ -2.5e-4 \\ 3.4e-4 \end{bmatrix}, \quad \boldsymbol{\sigma}_{\%\chi,full} = \begin{bmatrix} 0 \\ 2.43 \\ 0.92 \\ 0.05 \\ 0.14 \\ 0.16 \\ 0.46 \\ 107 \\ -22 \\ 23 \end{bmatrix}, \quad \sigma_W = 0.552, \quad C = 10.26 \quad (47)$$

Both experiments show cost function values very close to the absolute minimum, thus both of them provide optimal results in practice. The relative deviations of practically non-zero parameters, the *essential inertial parameters*, are well below the standard 10% threshold for acceptability. The only parameters estimated with very high relative standard deviations are the off-diagonal elements of the inertia matrix, which have indeed very low magnitude. These base parameters were then disregarded according to identification best practice, since they are *non-essential* [46]. The identification problems were then modified by removing the column of **W** corresponding to these parameters, but the value of previously well-identified parameters, as well as their relative standard deviations, changed negligibly.

By comparing the essential parameters identified by experiments with partial and full pose measurements, the following can be noticed:

- first, the accuracy of the results did not practically change: the same parameters are well identified with relative standard deviations far below 10%;

- second, the values of the essential parameters in $\boldsymbol{\chi}_{full}$ and $\boldsymbol{\chi}_{free}$, namely $\boldsymbol{\chi}^e_{full}$ and $\boldsymbol{\chi}^e_{free}$ [8], are comparable; if we compute the percentage relative error between $\boldsymbol{\chi}^e_{full}$ and $\boldsymbol{\chi}^e_{free}$ as:

$$\Delta \chi^e_{i,\%} = 100 \left\| \frac{\chi^e_{i,full} - \chi^e_{i,free}}{\chi^e_{i,free}} \right\| \% \quad (48)$$

and we compare them with $\boldsymbol{\sigma}^e_{\%\chi,free}$:

$$\boldsymbol{\sigma}^e_{\%\chi,free} = \begin{bmatrix} 0 \\ 4.32 \\ 3.09 \\ 0.15 \\ 0.64 \\ 0.31 \\ 1.76 \end{bmatrix}, \quad \Delta \boldsymbol{\chi}^e_{\%} = \begin{bmatrix} 0 \\ 21.14 \\ 0.01 \\ 0.76 \\ 1.11 \\ 0.04 \\ 2.77 \end{bmatrix} \quad (49)$$

we can conclude that the two results are equivalent in practice, since the relative errors between $\boldsymbol{\chi}^e_{full}$ and $\boldsymbol{\chi}^e_{free}$ are of the same order of magnitude of $\boldsymbol{\chi}^e_{free}$ standard deviations. The only parameter which is relatively different by comparison is the x coordinate

---

[8] Please note that essential parameters are the first 7 elements of both $\boldsymbol{\chi}_{full}$ and $\boldsymbol{\chi}_{free}$
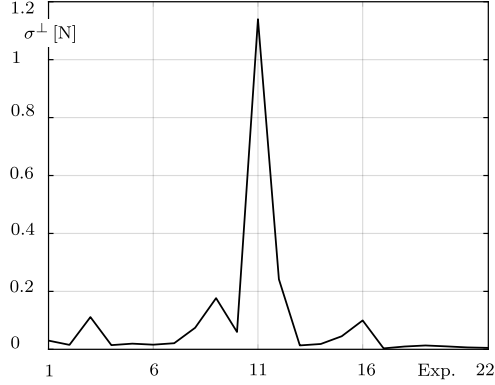
Figure 3: *Internal dynamics standard deviation in cross-validating experiments*

of the center of mass. On the other hand, the absolute difference of these components is 0.4mm, which is negligible in practice for an *EE* whose dimension is of the decimeter order.

In order to assess whether identification results are generally valid, 22 cross-validation free-motion experiments were conducted in random configurations (different from the ones used for identification), and the *EE* full pose was measured. Model error $\boldsymbol{\varepsilon} = \mathbf{W}\boldsymbol{\chi}$ was calculated for each experiment, with matrix $\mathbf{W}$ computed according to the measured data and $\boldsymbol{\chi}$ as in Eq. (46), and internal dynamics standard deviation $\sigma^\perp$ was calculated as:

$$\sigma^\perp = \sqrt{\frac{\boldsymbol{\varepsilon}^T \boldsymbol{\varepsilon}}{n_{cv}}} \tag{50}$$

370 with n_{cv} being the number of samples in the cross-validation experiments, $n_{cv} = 1001$. The values of $\sigma^\perp$ for the cross-validation experiments are reported in Fig. 3. The order of magnitude $\sigma^\perp$ for each experiment is near σ_W in Eq. (46) (only one experiment has $\sigma^\perp > \sigma_W$), thus identification results are validated.

Based on the experimental and cross-validating results, we can ultimately conclude that
375 (i) the use of the free-motion internal-dynamics identification model is effective in determining the *EE* base inertial parameters, and (ii) measuring the *EE* free coordinates and modelling its free motion, instead of measuring the full *EE* pose, does not negatively affect identification results, and thus it is a strong advantage of the proposed method.

6. Conclusions

380 This paper proposed a novel methodology for the identification of the inertial parameters of a *UACDPR EE*. This method, based on the use of internal-dynamics equations and free-motion excitations, and thereby called Free-Motion Internal-Dynamics Identification Model (*FIDIM*), was experimentally applied to a 4-cable *UACDPR*. Experimental results and cross validations showed a remarkable accuracy of the proposed technique. This method has the
385 merit of avoiding the use of force/torque measurements, which are required by state-of-the-art methods and usually negatively impact the identification procedure because of sensor noise. In addition, it was shown that any free-motion trajectory is optimal with respect to the

19

identification problem, thus there is no need to pre-compute it during experiment design. Lastly, it was shown that experimentation can be further simplified, by only measuring a sub-
390 set of the *EE* coordinates, the free ones, and modelling the *EE* free motion. These features both reduce identification equipment cost and simplify the identification procedure, while preserving the accuracy of results.

In the future, we will consider different optimal excitation strategies that can be fully auto-matic and do not require manual intervention: manual excitation of free-motion trajectories,
395 which is a limitation of the experimental validation of the proposed method, may not be eas-ily applied on real-world robots. Moreover, the external measuring device will be substituted with a pose estimation strategy that employs low-cost proprioceptive sensors.

References

[1] G. Mottola, C. Gosselin, M. Carricato, Effect of actuation errors on a purely-translational spatial cable-driven
400   parallel robot, in: 2019 IEEE 9th Annual International Conference on CYBER Technology in Automation, Con-trol, and Intelligent Systems (CYBER), 2019, pp. 701–707.

[2] E. Idà, T. Bruckmann, M. Carricato, Rest-to-rest trajectory planning for underactuated cable-driven parallel robots, IEEE Transactions on Robotics 35 (6) (2019) 1338–1351.

[3] E. Idà, S. Briot, M. Carricato, Natural oscillations of underactuated cable-driven parallel robots, IEEE Access 9
405   (2021) 71660–71672.

[4] J. W. Burdick, On the inverse kinematics of redundant manipulators: Characterization of the self-motion mani-folds, in: K. J. Waldron (Ed.), Advanced Robotics: 1989, Springer Berlin Heidelberg, Berlin, Heidelberg, 1989, pp. 25–34.

[5] J. Fink, N. Michael, S. Kim, V. Kumar, Planning and control for cooperative manipulation and transportation
410   with aerial robots, The International Journal of Robotics Research 30 (3) (2011) 324–334.

[6] L. Barbazza, D. Zanotto, G. Rosati, S. K. Agrawal, Design and optimal control of an underactuated cable-driven micro-macro robot, IEEE Robotics and Automation Letters 2 (2) (2017) 896–903.

[7] L. Scalera, A. Gasparetto, D. Zanotto, Design and experimental validation of a 3-dof underactuated pendulum-like robot, IEEE/ASME Transactions on Mechatronics 25 (1) (2020) 217–228.

415 [8] G. Abbasnejad, M. Carricato, Direct geometrico-static problem of underconstrained cable-driven parallel robots with *n* cables, IEEE Transactions on Robotics 31 (2) (2015) 468–478.

[9] A. Berti, J.-P. Merlet, M. Carricato, Solving the direct geometrico-static problem of underconstrained cable-driven parallel robots by interval analysis, The International Journal of Robotics Research 35 (6) (2016) 723–739.

[10] M. Carricato, J. Merlet, Stability Analysis of Underconstrained Cable-Driven Parallel Robots, IEEE Transactions
420   on Robotics 29 (1) (2013) 288–296.

[11] D. Surdilovic, J. Radojicic, Practical stability of under-constrained cable-suspended parallel robots, in: A. Pott, T. Bruckmann (Eds.), Cable-Driven Parallel Robots, Springer International Publishing, Cham, 2019, pp. 85–98.

[12] D. Cunningham, H. H. Asada, The winch-bot: A cable-suspended, under-actuated robot utilizing parametric self-excitation, in: 2009 IEEE International Conference on Robotics and Automation, 2009, pp. 1844–1850.

425 [13] N. Zoso, C. Gosselin, Point-to-point motion planning of a parallel 3-dof underactuated cable-suspended robot, in: 2012 IEEE International Conference on Robotics and Automation, 2012, pp. 2325–2330.

[14] J. Park, O. Kwon, J. H. Park, Anti-sway trajectory generation of incompletely restrained wire-suspended system, Journal of Mechanical Science and Technology 27 (10) (2013) 3171–3176.

[15] S. Lefrançois, C. Gosselin, Point-to-point motion control of a pendulum-like 3-dof underactuated cable-driven
430   robot, in: 2010 IEEE International Conference on Robotics and Automation, 2010, pp. 5187–5193.

[16] S. W. Hwang, J.-H. Bak, J. Yoon, J. H. Park, J.-O. Park, Trajectory generation to suppress oscillations in under-constrained cable-driven parallel robots, Journal of Mechanical Science and Technology 30 (12) (2016) 5689–5697.

[17] S. W. Hwang, J.-H. Bak, J. Yoon, J. H. Park, Oscillation reduction and frequency analysis of under-constrained
435   cable-driven parallel robot with three cables, Robotica (2019) 1–21.

[18] E. Idà, S. Briot, M. Carricato, Robust trajectory planning of under-actuated cable-driven parallel robot with 3 cables, in: J. Lenarčič, B. Siciliano (Eds.), Advances in Robot Kinematics 2020, Springer International Publishing, Cham, 2021, pp. 65–72.

[19] E. Idá, J.-P. Merlet, M. Carricato, Automatic self-calibration of suspended under-actuated cable-driven parallel
440   robot using incremental measurements, in: A. Pott, T. Bruckmann (Eds.), Cable-Driven Parallel Robots, Springer International Publishing, Cham, 2019, pp. 333–344.

[20] E. Idà, M. Carricato, A new performance index for underactuated cable-driven parallel robots, in: M. Goutte-farde, T. Bruckmann, A. Pott (Eds.), Cable-Driven Parallel Robots, Springer International Publishing, 2021, pp. 24–36.

[21] R. de Rijk, M. Rushton, A. Khajepour, Out-of-plane vibration control of a planar cable-driven parallel robot, IEEE/ASME Transactions on Mechatronics 23 (4) (2018) 1684–1692.

[22] M. Zarei, A. Aflakian, A. Kalhor, M. T. Masouleh, Oscillation damping of nonlinear control systems based on the phase trajectory length concept: An experimental case study on a cable-driven parallel robot, Mechanism and Machine Theory 126 (2018) 377 – 396.

[23] M. R. Jafari Harandi, H. Damirchi, S. a. Khalilpour seyedi, H. D. Taghirad, Point-to-point motion control of an underactuated planar cable driven robot, in: 2019 27th Iranian Conference on Electrical Engineering (ICEE), 2019, pp. 979–984.

[24] H. Jamshidifar, M. Rushton, A. Khajepour, A reaction-based stabilizer for nonmodel-based vibration control of cable-driven parallel robots, IEEE Transactions on Robotics 37 (2) (2021) 667–674.

[25] S. Briot, M. Gautier, Global identification of joint drive gains and dynamic parameters of parallel robots, Multi-body System Dynamics 33 (1) (2015) 3–26.

[26] M. Gautier, Numerical calculation of the base inertial parameters of robots, Journal of Robotic Systems 8 (4) (1991) 485–506.

[27] R. Chellal, E. Laroche, L. Cuvillon, J. Gangloff, An identification methodology for 6-dof cable-driven parallel robots parameters application to the INCA 6D robot, in: T. Bruckmann, A. Pott (Eds.), Cable-Driven Parallel Robots, Springer Berlin Heidelberg, Berlin, Heidelberg, 2013, pp. 301–317.

[28] R. Chellal, L. Cuvillon, E. Laroche, Model identification and vision-based h∞ position control of 6-dof cable-driven parallel robots, International Journal of Control 90 (4) (2017) 684–701.

[29] P. Tempel, P. Herve, O. Tempier, M. Gouttefarde, A. Pott, Estimating inertial parameters of suspended cable-driven parallel robots — use case on CoGiRo, in: 2017 IEEE International Conference on Robotics and Automation (ICRA), 2017, pp. 6093–6098.

[30] W. Kraus, V. Schmidt, P. Rajendra, A. Pott, System identification and cable force control for a cable-driven parallel robot with industrial servo drives, in: 2014 IEEE International Conference on Robotics and Automation (ICRA), 2014, pp. 5921–5926.

[31] M. Gobbi, G. Mastinu, G. Previati, A method for measuring the inertia properties of rigid bodies, Mechanical Systems and Signal Processing 25 (1) (2011) 305 – 318.

[32] L. Tang, W.-B. Shangguan, An improved pendulum method for the determination of the center of gravity and inertia tensor for irregular-shaped bodies, Measurement 44 (10) (2011) 1849 – 1859.

[33] G. Previati, M. Gobbi, G. Mastinu, Measurement of the mass properties of rigid bodies by means of multi-filar pendulums – influence of test rig flexibility, Mechanical Systems and Signal Processing 121 (2019) 31 – 43.

[34] G. Previati, Large oscillations of the trifilar pendulum: Analytical and experimental study, Mechanism and Machine Theory 156 (2021) 104157.

[35] W. Khalil, E. Dombre, Modeling, identification and control of robots, Butterworth-Heinemann, 2004.

[36] C. I. Byrnes, A. Isidori, Local stabilization of minimum-phase nonlinear systems, Systems & Control Letters 11 (1) (1988) 9–17.

[37] A. De Luca, Zero dynamics in robotic systems, in: C. I. Byrnes, A. B. Kurzhansky (Eds.), Nonlinear Synthesis: Proceedings of a IIASA Workshop held in Sopron, Hungary June 1989, Cable-Driven Parallel Robots, Birkhäuser Boston, Boston, MA, 1991, pp. 68–87.

[38] S. Van Huffel, J. Vandewalle, The total least squares problem: computational aspects and analysis, SIAM, 1991.

[39] J. Nocedal, S. Wright, Numerical optimization, Springer Science & Business Media, 2006.

[40] M. Conconi, M. Carricato, A new assessment of singularities of parallel kinematic chains, IEEE Transactions on Robotics 25 (4) (2009) 757–770.

[41] G. Oriolo, Y. Nakamura, Control of mechanical systems with second-order nonholonomic constraints: under-actuated manipulators, in: 30th IEEE Conference on Decision and Control, 1991, pp. 2398–2403.

[42] A. Pott, Cable-driven parallel robots: theory and application, Vol. 120, Springer, 2018.

[43] Cong Bang Pham, Guilin Yang, Song Huat Yeo, Dynamic analysis of cable-driven parallel mechanisms, in: Proceedings, 2005 IEEE/ASME International Conference on Advanced Intelligent Mechatronics., 2005, pp. 612–617.

[44] M. Gautier, S. Briot, Global Identification of Joint Drive Gains and Dynamic Parameters of Robots, Journal of Dynamic Systems, Measurement, and Control 136 (5), 051025.

[45] M. Gautier, Dynamic identification of robots with power model, in: Proceedings of International Conference on Robotics and Automation, Vol. 3, 1997, pp. 1922–1927 vol.3.

[46] C. Pham, M. Gautier, Essential parameters of robots, in: [1991] Proceedings of the 30th IEEE Conference on Decision and Control, 1991, pp. 2769–2774 vol.3.

[47] M. Gautier, W. Khalil, Exciting trajectories for the identification of base inertial parameters of robots, International Journal of Robotics Research 11 (4) (1992) 362–375.

21

[48] J. Jin, N. Gans, Parameter identification for industrial robots with a fast and robust trajectory design approach, Robotics and Computer-Integrated Manufacturing 31 (2015) 21 – 29.

[49] V. Bonnet, P. Fraisse, A. Crosnier, M. Gautier, A. González, G. Venture, Optimal exciting dance for identifying inertial parameters of an anthropomorphic structure, IEEE Transactions on Robotics 32 (4) (2016) 823–836.

[50] J. Swevers, W. Verdonck, J. De Schutter, Dynamic model identification for industrial robots, IEEE Control Systems Magazine 27 (5) (2007) 58–71.

[51] M. Gautier, P. O. Vandanjon, C. Presse, Identification of inertial and drive gain parameters of robots, in: Proceedings of 1994 33rd IEEE Conference on Decision and Control, Vol. 4, 1994, pp. 3764–3769.

[52] C. Presse, M. Gautier, New criteria of exciting trajectories for robot identification, in: Proceedings IEEE International Conference on Robotics and Automation, Vol. 3, 1993, pp. 907–912.

[53] G. H. Golub, C. F. Van Loan, Matrix computations, 4th, Johns Hopkins.

[54] T. Katsumata, B. Navarro, V. Bonnet, P. Fraisse, A. Crosnier, G. Venture, Optimal exciting motion for fast robot identification. Application to contact painting tasks with estimated external forces, Robotics and Autonomous Systems 113 (2019) 149 – 159.

[55] J.-P. Merlet, Direct kinematics of cdpr with extra cable orientation sensors: The 2 and 3 cables case with perfect measurement and ideal or elastic cables, in: C. Gosselin, P. Cardou, T. Bruckmann, A. Pott (Eds.), Cable-Driven Parallel Robots, Springer, Cham, 2018, pp. 180–191.